PAPER

CrossMark
click for updates

Gd₃Ni₂ and Gd₃CoₓNi₂₋ₓ: magnetism and unexpected Co/Ni crystallographic ordering†

Alessia Provino,*[abc] Volodymyr Smetana,[ad] Durga Paudyal,[a]
Karl A. Gschneidner Jr,[ad] Anja-Verena Mudring,[ad] Vitalij K. Pecharsky,[ad]
Pietro Manfrinetti[abc] and Marina Putti[ce]

The crystal structure, composition and physical properties of Gd₃Ni₂, which was earlier reported to exist in the Gd–Ni system without any details of its structure and properties, have been determined. This rare earth binary compound is a high-temperature phase: it forms *via* a peritectic reaction at 988 K (715 °C) and decomposes below $\approx$923 K (650 °C). The compound can be retained at room temperature as a metastable phase by quenching after high temperature annealing. Gd₃Ni₂ crystallizes in the monoclinic Dy₃Ni₂ structure type [mS20, C2/m (No. 12), Z = 4; with lattice parameters a = 13.418(3) Å, b = 3.720(1) Å, c = 9.640(2) Å, β = 106.250(3)°]. Ni can be substituted by Co up to 50% (*i.e.* up to and including Gd₃CoNi) with no change in the structural prototype; the substitution of Co for Ni stabilizes the R₃CoₓNi₂₋ₓ phases down to room temperature. The crystal structure, magnetic properties and magnetocaloric effect (MCE) have been investigated for both Gd₃Ni₂ and the related Gd₃CoₓNi₂₋ₓ solid solution alloys (0 ≤ x ≤ 1). The crystal structure of the Gd₃CoNi is a ternary ordered derivative of the monoclinic Dy₃Ni₂-type, where Co fully occupies only one of the two 4i Wyckoff sites available for the transition metal. To the best of our knowledge, this is the first example of an intermetallic phase showing ordered site occupations by the chemically quite similar elements Co and Ni. All compounds show long range ferromagnetic ordering, with T_C progressively increasing from 147 K (for Gd₃Ni₂) to 176 K (for Gd₃CoNi) as a cubic function of the Co content. Evidence of Co contributing to the magnetic interactions in these compounds has been found. First-principles total energy calculations predicted the ordered occupation of Co and Ni at the crystallographic sites of Gd₃CoNi, which was later confirmed by single crystal X-ray diffraction. The increased conduction electronic state (3d) exchange splitting at the Fermi level supports the experimentally observed enhanced Curie temperature in Gd₃CoNi compared to Gd₃Ni₂.

1 Introduction

Systematic research on new semi-metallic and metallic phases as potential functional materials for advanced technological applications has been and still remains a tremendously important field of study for solid state chemistry, condensed matter physics,

[a] *The Ames Laboratory, U.S. Department of Energy, Division of Materials Sciences and Engineering, Iowa State University, Ames, IA 50011-3020, USA. E-mail: alessia.provino@spin.cnr.it*
[b] *Department of Chemistry, University of Genova, Via Dodecaneso 31, 16146 Genova, Italy*
[c] *Institute SPIN-CNR, Corso Perrone 24, 16152 Genoa, Italy*
[d] *Department of Materials Science and Engineering, Iowa State University, Ames, IA 50011-2300, USA*
[e] *Department of Physics, University of Genova, Via Dodecaneso 33, 16146 Genova, Italy*
† Electronic supplementary information (ESI) available. CCDC 1458711 and 1458712. For ESI and crystallographic data in CIF or other electronic format see DOI: 10.1039/c6tc01035k

and materials science and engineering communities. A substantial body of work is concerned with the improvement of mechanical (hardness, high tensile strength), chemical (biocompatibility, oxidation and corrosion resistance), and physical properties (thermal and electrical conductivity, magnetism) of already known materials and/or the search for new materials with interesting properties.[1,2] In this context, while binary phases have already been studied for many years, ternary and quaternary systems attract most interest at the present time. Among them, intermetallic compounds formed by rare earth (R), transition (M), and p-block elements are relatively well investigated, mainly because of their diverse magnetic properties that include hard or soft ferromagnetism, giant magnetostriction, and the giant magnetocaloric effect. The search for new materials with an enhanced magnetocaloric effect (MCE) and large refrigerant capacity (RC) that can be used in room- and low-temperature magnetocaloric refrigerators is one of the current research topics driven by the expected low energy consumption and low environmental impact of these devices.[3] While room temperature

6078 | *J. Mater. Chem. C*, 2016, 4, 6078–6089

This journal is © The Royal Society of Chemistry 2016

magnetocaloric refrigerant materials may find applications in air conditioners and household refrigerators, low temperature materials are equally important due to their potential use, for example, in the energy efficient liquefaction of natural gas and hydrogen. Rare earth based compounds and Gd intermetallics have been proven in general to possess large MCEs.[2,3]

Despite a large number of known binary R–M compounds, there remain quite a few binary systems with reported but not fully investigated compounds. To mention some, '$Nd_2Co_{1.7}$', 'Gd_3Ni_2', 'Lu_2Pd_5', and 'R_2Pd_3', and 'RPd_2' (R = rare earth)[4–6] remain listed with uncertain compositions and unknown crystal structures. In the Gd–Ni binary system, a total of nine compounds have been reported to exist: Gd_2Ni_{17}, $GdNi_5$, $GdNi_4$, Gd_2Ni_7 (high- and low-temperature polymorphs), $GdNi_3$, $GdNi_2$, $GdNi$, Gd_3Ni_2 and Gd_3Ni.[4–7] The crystal structure has been determined for all of them except for '$GdNi_4$' and 'Gd_3Ni_2'. The 'Gd_3Ni_2' phase was reported to form by a peritectic reaction at 690 °C with no additional structural details; a tetragonal cell with lattice parameters a = 7.28 Å and c = 8.61 Å has been proposed for this compound.[8] However, more recent work indicated that '$GdNi_4$' and 'Gd_3Ni_2' do not exist,[9] in apparent agreement with an earlier paper on this system.[7] However, stoichiometric phases of composition R_3Ni_2 have been detected for R = Tb, Dy, Ho, Er, and Y; all of them form by a peritectic reaction (liquid + RNi). Tb_3Ni_2 and Dy_3Ni_2 are known to crystallize in the monoclinic Dy_3Ni_2-type [Pearson symbol $mS20$, space group $C2/m$ (No. 12), $Z = 4$],[10] while Er_3Ni_2 and Y_3Ni_2 crystallize in their own prototypes: the hexagonal Er_3Ni_2 [$hR45$, $R\bar{3}$ (No. 148), $Z = 9$],[11] and tetragonal Y_3Ni_2 [$tP80$, $P4_12_12$ (No. 92), $Z = 16$],[12] respectively. Ho_3Ni_2 is reported to be dimorphic, adopting the hexagonal Er_3Ni_2-type [the high-temperature (HT) form] and the Dy_3Ni_2-type [the low-temperature (LT) form].[10] Since the existence of the 'Gd_3Ni_2' phase remains doubtful, yet such a material would be of potential interest as a magnetic refrigerant material, a thorough investigation of its formation and stoichiometry is warranted.[13]

In this work we report the crystal structure, thermal stability, magnetic behavior and magnetocaloric effect (MCE) of Gd_3Ni_2 and substituted $Gd_3Co_xNi_{2-x}$ phases for $0 < x \leq 1.0$. Electronic structure calculations have been performed to understand the preferential Co/Ni site occupations leading to the confirmation of the ternary Gd_3CoNi ordered derivative and the magnetic behaviors of these compounds.

2 Experimental section

Materials synthesis

Polycrystalline samples (each about 5 g total mass), with nominal composition Gd_3Ni_2 and $Gd_3Co_xNi_{2-x}$ (with x = 0.25, 0.50, 0.75, 0.85, 0.95, 1.00), were synthesized by arc melting the elements weighed in stoichiometric proportions under an Ar atmosphere. The starting constituents were high purity Gd (99.9 + wt% purity) obtained from the Materials Preparation Center of the Ames Laboratory,[14] and commercial Co and Ni (both 99.99 wt% purity). The buttons were melted at least three times, turning them

upside down to ensure homogeneity. Weight losses after the melting were less than 0.2%. A TiZr getter was melted and then solidified prior to melting the samples in order to ensure a clean atmosphere in the arc-furnace chamber. The ingots were wrapped in a Ta foil, sealed under vacuum in quartz tubes, annealed at 953–973 K for 7–10 days, and then quenched in water.

X-ray diffraction studies

Phase analyses and structural characterization were performed by X-ray powder diffraction (XRD) using both a PANanalytical X'Pert diffractometer (Cu Kα_1 radiation) and a Guinier camera (Cu Kα_1 radiation); the X-ray patterns were indexed with the help of Lazy PULVERIX[15] and lattice parameters were refined by means of least-square methods. The microstructure and homogeneity of the alloys were checked by optical microscopy and scanning electron microscopy complemented by a microprobe for semi-quantitative analysis (SEM-EDX) [Leica Cambridge 360 microscope, equipped with an Oxford X-Max 20 analyzer; work parameters: EHT 20.0 kV and probe current 220 pA (Oxford Aztec software)]. Single crystal X-ray diffraction data were collected using crystals measuring ≈ 60–120 μm, selected under a microscope from the annealed Gd_3Ni_2 and Gd_3CoNi alloys and checked by the Laue method. The intensity data were collected at 293 K on a Bruker APEX CCD diffractometer (Mo Kα radiation) in φ- and ω-scan modes using at least 1200 frames and an exposure of 15 s per frame. The intensities of the Bragg reflections were integrated using the SAINT program in the SMART software package.[16] The space group determination was achieved employing the XPREP algorithms within the SHELXTL program suite.[17] The structure solution was accomplished by direct methods using SIR-97,[18] and subsequent structure refinement was carried out using SHELX-97.[19]

Thermal analysis

Differential thermal analysis (DTA) was performed by using a Netzsch 404 apparatus on selected bulk samples (0.7–0.9 g), either as cast or annealed, sealed in an outgassed Mo crucible under an Ar atmosphere. Data were recorded upon heating at 20 K min^{-1} and upon cooling at 10 K min^{-1} (accuracy ±5 K). Differential scanning calorimetry (DSC) was carried out on a Netzsch STA 449F3 apparatus (0.4 g specimens); thermal cycles were generally carried out at rates of 20 K min^{-1} both upon heating and cooling. The accuracy in the temperature measurement was of ±1 K.

Physical property measurements

The magnetization measurements were carried out using a Magnetic Properties Measurement System (SQUID, Quantum Design). Magnetization as a function of temperature was measured between 2 and 300 K and under applied magnetic fields of 200 Oe and 2 kOe; isothermal magnetization was measured at various temperatures in applied fields up to 70 kOe. Magnetocaloric effect, MCE, was calculated from isothermal magnetization measurements recorded around the magnetic transition temperatures at intervals of 5 K in applied fields up to 50 kOe. Heat capacity data were

This journal is © The Royal Society of Chemistry 2016

J. Mater. Chem. C, 2016, **4**, 6078–6089 | **6079**

collected for Gd_3Ni_2 (between 2 K and 300 K and in applied magnetic fields of 0, 10, 20, 30, 40 and 50 kOe) and for $Gd_3Co_{0.5}Ni_{1.5}$ (between 77 K and 300 K and in fields of 10 and 20 kOe) using a home built automated adiabatic calorimeter.[20]

3 Results and discussion

3.1 Formation and stability of Gd_3Ni_2 and $Gd_3Co_xNi_{2-x}$

Gd_3Ni_2 is a high-temperature phase that exists in a narrow temperature interval ($\approx$ 65 K). While the coexistence of three phases [GdNi (CrB-type, $oP8$, $Pnma$), Gd_3Ni (Fe_3C-type, $oP16$, $Pnma$), and Gd_3Ni_2, according to the X-ray powder diffraction and SEM-EDX analysis] was observed in the as-cast samples (Fig. S1, ESI†), those annealed at or below 923 K contained only the two known binary compounds GdNi and Gd_3Ni. Several annealing treatments at temperatures between 923 K and 973 K, followed by quenching, were attempted in order to determine the formation and decomposition temperatures of Gd_3Ni_2. Samples quenched after heat treatment between 933 K and 973 K were obtained as single phase products, containing only the stoichiometric Gd_3Ni_2 compound. Single phase samples are highly crystalline, brittle, and only slightly sensitive to air. To determine the formation temperature, DTA analyses were performed on as-cast and annealed Gd_3Ni_2 samples. The data showed that the Gd_3Ni_2 phase forms by a peritectic reaction (liquid + GdNi → Gd_3Ni_2) at 988 K, but they did not allow us to clearly identify the eutectoid decomposition temperature (2 Gd_3Ni_2 → 3 GdNi + Gd_3Ni). Gd_3Ni_2 can be preserved at room temperature as a metastable phase through quenching from high temperature.

The X-ray powder patterns were indexed, with the help of Lazy PULVERIX,[15] on the basis of the monoclinic Dy_3Ni_2 prototype [$mS20$, $C2/m$ (No. 12), $Z = 4$].[10] The lattice parameters (a, b, c, and β), unit cell volume (V_{obs}) and volume of formation $\{-\Delta V \%$, where $\Delta V = [(V_{calc} - V_{obs})/V_{calc} \times 100]$; V_{calc} is the volume of the compound calculated from the atomic volumes of the individual atoms[21]$\}$ for Gd_3Ni_2 are reported in Table 1. The lattice parameters are larger than those of the other known Dy_3Ni_2-type R_3Ni_2 phases (R = Tb, Dy, hT-Ho),[10] and are in agreement with the trend of the lanthanide contraction. The volume of formation observed for Gd_3Ni_2 ($\approx -4.7\%$) is relatively small compared to the values obtained for other Gd–Ni compounds and several binary and ternary Gd phases,[5,6] suggesting

that a considerably low atomic space filling takes place in the formation of this compound. This result prompted us either to investigate pseudo-binary alloys by substituting either Gd by a larger R (e.g. Nd), or Ni by a larger transition element (e.g. Co, Pd), or by the addition of a small interstitial element (e.g. B, C), to check if the Dy_3Ni_2 structure type was preserved, and if the substitution could stabilize the formation of this phase. Co substitution was first attempted because of its similarity to Ni (the atomic volumes are 11.08 Å^3 and 10.93 Å^3 for Co and Ni, respectively[21]). Samples with nominal composition $Gd_3Co_xNi_{2-x}$ (for x = 0.25, 0.50, 0.75, 0.85, 0.95, 1.00) were prepared and studied. As a first result, we found that the Co substitution for Ni stabilizes the pseudo-binary $Gd_3Co_xNi_{2-x}$ phases down to room temperature; the alloy with the lowest Co content, i.e. $Gd_{60}Co_5Ni_{35} \equiv Gd_3Co_xNi_{2-x}$ with x = 0.25 was still a single phase with the Dy_3Ni_2-type structure after annealing at 673 K (well below the eutectoid decomposition temperature of pure Gd_3Ni_2) for 18 days. An X-ray powder diffraction pattern of $Gd_{60}Co_{15}Ni_{25}$, along with its Rietveld profile, is shown as an example in Fig. 1. Moreover, the monoclinic prototype is preserved up to the composition Gd_3CoNi (x = 1.0). When x exceeds 1, the crystal structure changes to the orthorhombic Y_3Co_2 prototype [$oP20$, $Pnnm$ (No. 58), Z = 4]. The two prototypes – Dy_3Ni_2 and Y_3Co_2 – are closely related to one another via displacements of slabs common to both structures,[22] which are similar to the relationships between CrB-,
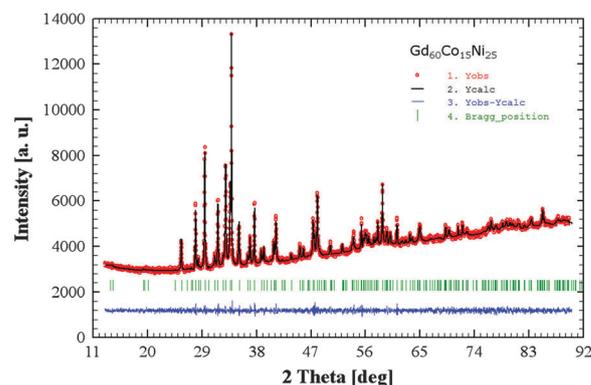

Fig. 1 Observed X-ray powder pattern (red circles) and the Rietveld refinement profile (black line) for the sample with nominal composition $Gd_{60}Co_{15}Ni_{25}$. The lower profile (blue line) is the difference between the observed and calculated data; the Bragg angle positions are indicated by vertical bars (green).

Table 1 Lattice parameters (a, b, c, and β), unit cell volume (V_{obs}), mean atomic volume (V_{at}) and volume of formation ($-\Delta V \%$) for Gd_3Ni_2 and the $Gd_3Co_xNi_{2-x}$ compounds [Dy_3Ni_2-type, $mS20$, $C2/m$ (No. 12)]

$Gd_3Co_xNi_{2-x}$	Co [at%]	Lattice parameters				V_{obs} [Å^3]	V_{at} [Å^3]	$-\Delta V$ [%]
		a [Å]	b [Å]	c [Å]	β [°]			
Gd_3Ni_2	0	13.419(3)	3.720(1)	9.640(2)	106.250(3)	461.97	23.10	4.68
$Gd_3Co_{0.25}Ni_{1.75}$	5	13.420(2)	3.7358(5)	9.6000(9)	106.738(11)	460.90	23.04	4.93
$Gd_3Co_{0.50}Ni_{1.50}$	10	13.4160(9)	3.7529(3)	9.5708(5)	107.385(5)	459.87	22.99	5.17
$Gd_3Co_{0.75}Ni_{1.25}$	15	13.408(1)	3.7796(5)	9.5464(5)	108.128(7)	459.78	22.99	5.22
$Gd_3Co_{0.85}Ni_{1.15}$	17	13.405(1)	3.7895(6)	9.537(1)	108.481(8)	459.50	22.97	5.29
$Gd_3Co_{0.95}Ni_{1.05}$	19	13.402(2)	3.803(1)	9.534(1)	108.828(2)	459.89	22.99	5.22
Gd_3CoNi	20	13.400(2)	3.810(1)	9.537(2)	109.028(2)	460.33	23.02	5.13

Lattice parameters for Gd_3Ni_2 are those from a sample annealed at 953 K for 6 days and quenched in water.

6080 | J. Mater. Chem. C, 2016, **4**, 6078–6089

This journal is © The Royal Society of Chemistry 2016

FeB-, and TbNi-type structures. All the substituted $Gd_3Co_xNi_{2-x}$ phases also form *via* peritectic reactions, at temperatures slightly, but progressively, decreasing with increasing Co content [from 988 K (715 °C) for Gd_3Ni_2 to 981 K (708 °C) for $Gd_3Co_{0.75}Ni_{1.25}$ and 975 K (702 °C) for Gd_3CoNi]. A DSC trace for Gd_3CoNi alloy is shown in Fig. S1 in the ESI.†

In $Gd_3Co_xNi_{2-x}$ both a and c decrease, while b and β increase with x, and the unit cell volume slightly decreases (Fig. 2, Table 1). Since the atomic volume of elemental Co is slightly larger than that of Ni, one would have expected the opposite – an increase of the unit cell volume with increasing Co content. The observed decrease may be due to either the fact that Co assumes an anomalously large volume in its elemental form, and when alloyed it behaves as a normal 3d metal with a smaller atomic volume than Ni,[23] or to the peculiar site preference of Co atoms (see next section). The absolute value of the volume of formation ($|\Delta V|$ %) in these compounds sensibly increases with the Co content (Fig. 2); since the volume of formation is proportional to the thermodynamic stability (heat of formation) of the compound,[24,25] such an increase across the $Gd_3Co_xNi_{2-x}$ series supports the notion of a higher stability brought about as a result of Co substitutions. At the same time, the trends illustrated in Fig. 2 suggest that the unit cell will not sustain a higher Co substitution while preserving the same monoclinic Dy_3Ni_2-type structure. A structural change to the orthorhombic Y_3Co_2-type for $x > 1.0$ is in fact observed; this will be the subject of a future study.

3.2 Crystal structure of Gd₃Ni₂ and Gd₃CoNi

Single crystal X-ray structure analysis confirms the monoclinic Dy_3Ni_2-type structure [$mS20$, $C2/m$ (No. 12), $Z = 4$][10] for both Gd_3Ni_2 and Gd_3CoNi. Five crystallographically independent atomic positions are present in the Dy_3Ni_2-type; all have the Wyckoff symbol 4i with two independent coordinates ($x\ 0\ z$).[26] The structure (Fig. 3a and c) is characterized by strands of *trans*-triangular face sharing trigonal prisms of Dy centered by Ni atoms; four of these strands are condensed through shared *cis*-rectangular faces to form columns of four face-sharing slabs along the *b*-axis (the shortest axis). Due to this the coordination sphere around Ni is enlarged to the form of a distorted tricapped trigonal prism (CN = 9) with two transition metals and one gadolinium atom capping the trigonal Gd prism around Ni. The atomic coordination around the Gd atoms features large and distorted polyhedra with high coordination numbers (CN = 14, 16, 17), typical of intermetallic phases. The crystal data and structure refinement details are collected in Table 2, the atomic parameters are reported in Table 3 and Fig. S1 (ESI†), while the interatomic distances are listed in Tables S2 and S3 (ESI†) for Gd_3Ni_2 and Gd_3CoNi, respectively. The single crystal structure refinement suggested the strong site preference for the Co atoms in the solid solution. Although conventional scattering factors of Co and Ni are only different by a single electron (less than 4%), crystallographic (next paragraph) and geometrical analyses, as well as total energy calculations for different coloring models (Section 3.4), are in favor of all sites in Gd_3CoNi being ordered and fully occupied. Hence, this is a

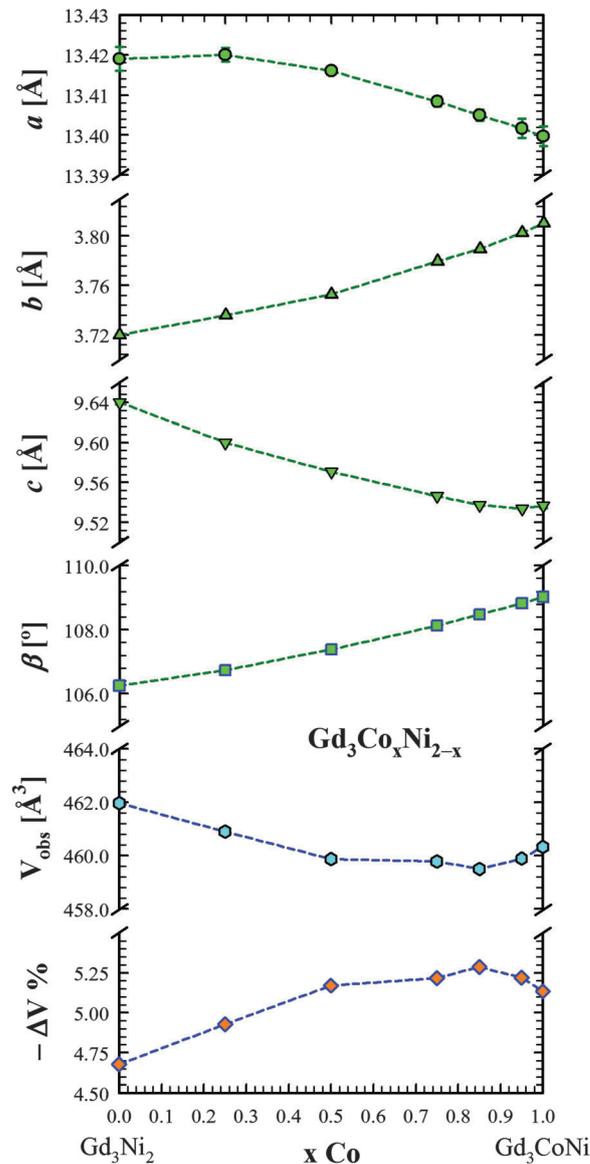**Fig. 2** The trends of the lattice parameters (*a*, *b*, *c*, and *β*), unit cell volume (V_{obs}), and volume of formation ($-\Delta V$ %) *vs.* the Co content in the $Gd_3Co_xNi_{2-x}$ compounds (x = 0, 0.25, 0.50, 0.75, 0.85, 0.95, 1.00); the dashed lines are guides to the eye.

true stoichiometric ternary compound, whose crystal structure represents a new ternary prototype, an ordered derivative of the Dy_3Ni_2-type (Fig. 3b and d).

Because of their close electronegativities (1.88 for Co and 1.91 for Ni, Pauling scale) and atomic size, Co and Ni frequently occupy the same crystallographic sites forming solid solutions leading generally to fully or partially disordered structures. The high quality of the Gd_3CoNi crystals allowed us to distinguish fully occupied Co and Ni positions. Slightly better *R*-values (statistically significant, according to the Hamilton test[27]) and, more importantly, uniform thermal displacement parameters were obtained by setting Ni and Co as listed in Table 3. The opposite distribution of Ni and Co (different coloring scheme) leads to $U_{eq} = 0.0160(7)$ and $0.0207(6)$ for Co and Ni, respectively.
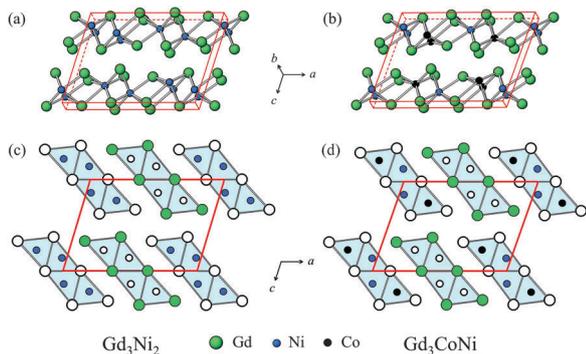
Fig. 3 Sketch of the crystal structure of Gd_3Ni_2 (a) and Gd_3CoNi (b), where only the shortest Gd–Ni and Gd–Co interatomic distances are depicted, respectively. Projection of the crystal structure of Gd_3Ni_2 (c) and Gd_3CoNi (d) along the b-axes, where the trigonal-prismatic arrangement is shown.

Table 3 Standardized fractional atomic coordinates and equivalent displacement parameters of Gd_3Ni_2 and Gd_3CoNi. All atoms are in 4i (x 0 z). The isotropic displacement parameter, U_{eq}, is defined as one third of the trace of the orthogonalized U_{ij} tensor

Atom	Atomic coordinates			U_{eq} [Å²]
	x	y	z	
Gd_3Ni_2				
Gd1	0.36797(9)	0	0.0018(1)	0.0157(3)
Gd2	0.0971(1)	0	0.6728(1)	0.0164(3)
Gd3	0.35598(9)	0	0.6295(1)	0.0167(3)
Ni1	0.03578(3)	0	0.1432(3)	0.0210(7)
Ni2	0.24231(3)	0	0.2268(3)	0.0220(7)
Gd_3CoNi				
Gd1	0.36691(8)	0	0.0009(1)	0.0106(4)
Gd2	0.10373(9)	0	0.6773(1)	0.0118(4)
Gd3	0.36179(8)	0	0.6260(1)	0.0115(4)
Ni	0.0354(3)	0	0.1425(4)	0.0173(7)
Co	0.2378(2)	0	0.2371(4)	0.0161(7)

In the intermediate $Gd_3Co_xNi_{2-x}$ phases, Co gradually replaces Ni at the Ni2 site of the parent compound, up to the full occupancy in Gd_3CoNi; hence the 3:1:1 stoichiometric compound corresponds to the Co-rich limit of the series adopting the Dy_3Ni_2-type. Since the difference in atomic size and electronegativity between Ni and Co is nearly negligible, the crystallographic ordering of these atoms must be primarily controlled by the electronic factors.

A sketch of the crystal structure of both Gd_3Ni_2 and Gd_3CoNi compounds is shown in Fig. 3a and b, respectively, where the ordered arrangement of the Co atoms is highlighted. The structure is represented by a trigonal-prismatic arrangement of the smaller atoms, forming columns of four face-sharing

blocks along the shortest crystallographic axis, b. The trigonal prisms are centered by Ni atoms in Gd_3Ni_2, or by Co/Ni atoms in Gd_3CoNi (Fig. 3c and d).

A comparison of the interatomic distances indicates that some values clearly decrease in Gd_3CoNi when compared to Gd_3Ni_2 (Tables S2 and S3, ESI†). Since all these values are lower than the sum of their corresponding metallic radii, $\sum r_M$, (where $r_M = 1.802$ Å, 1.252 Å and 1.246 Å for Gd, Co and Ni, respectively),[28] it is reasonable to consider them as bond distances. The shortest Gd2–Ni2 distance in the Gd_3Ni_2 structure $\delta_{Gd_2-Ni_2} = 2.809$ Å (−7.8%) contracts to $\delta_{Gd_2-Co} = 2.771$ Å (−9.3%) in Gd_3CoNi. The shortest Gd–Gd interatomic distances, 3.548–3.727 Å for Gd_3Ni_2 (−1.6% to +3.4% with respect $2r_{Gd} = 3.604$ Å) and 3.574–3.854 Å for

Table 2 Crystal data and structure refinement details for Gd_3Ni_2 and Gd_3CoNi at $T = 293(2)$ K

Compound	Gd_3Ni_2	Gd_3CoNi
Structure prototype	Dy_3Ni_2	Dy_3Ni_2
Pearson code	$mS20$	$mS20$
Crystal system	Monoclinic	Monoclinic
Space group	$C2/m$ (No. 12)	$C2/m$ (No. 12)
Lattice parameters	$a = 13.445(3)$ Å	$a = 13.407(2)$ Å
	$b = 3.7270(7)$ Å	$b = 3.8118(7)$ Å
	$c = 9.646(2)$ Å	$c = 9.5351(19)$ Å
	$\beta = 106.44(3)°$	$\beta = 109.079(10)°$
Unit cell volume [Å³]	463.6(2)	460.51(14)
Unit formula per cell, Z	4	4
Absorption coefficient, μ (Mo Kα) [mm⁻¹]	50.078	49.927
Calculated density, ρ [g cm⁻³]	8.441	8.501
$F(000)$	992	988
Crystal size [mm]	0.08 × 0.06 × 0.06	0.11 × 0.08 × 0.12
Theta range [°]	$3.16 \leq \theta \leq 26.66$	$2.26 \leq \theta \leq 27.50$
Range in h, k, l	$-15 \leq h \leq 15, -4 \leq k \leq 4, 0 \leq l \leq 12$	$-17 \leq h \leq 17, -4 \leq k \leq 4, -11 \leq l \leq 12$
Measured reflections	900	1659
Independent reflections	527	597
Absorption correction	Empirical	Empirical
Refinement method	Full-matrix least-squares on F^2	Full-matrix least-squares on F^2
Refined parameters	32	32
Data/restraints/parameters	527/0/32	597/0/32
$R1$ all data, w$R2$ (F_o^2) all data	0.0619, 0.0685	0.0389, 0.1096
$R1$, w$R2$ (F_o^2) [$I > 2\sigma(I)$]	0.0379, 0.0633	0.0315, 0.0755
R_{int}	0.035	0.029
Goodness-of-fit	1.037	1.234
$\Delta\rho_{max}$, $\Delta\rho_{min}$, e Å⁻³	+1.925, −2.815	+2.605, −2.196

6082 | *J. Mater. Chem. C*, 2016, **4**, 6078–6089

This journal is © The Royal Society of Chemistry 2016

Gd_3CoNi (-2.8% to $+5.8\%$, respectively), show relatively weak Gd–Gd interactions. Upon the transition from Gd_3Ni_2 to Gd_3CoNi, the Gd1–Gd2 and Gd1–Gd3 distances decrease from 4.098 Å to 3.854 Å and from 4.353 Å to 4.175 Å, respectively, while the Gd1–Gd1, Gd2–Gd2, and Gd3–Gd3 increase from 3.727 Å to 3.812 Å; the other Gd–Gd distances remain practically constant ($<1.2\%$). Weak Ni–Ni, or Ni–Co, chemical bonds are also formed in both compounds (Tables S2 and S3, ESI†).

To better understand the distribution of the neighboring atoms around Gd, Co and Ni in these two phases, we used criteria described by Bruzzone *et al.*[29] In this approach, the atomic distribution around one given atom is described by plotting the number of its surrounding atoms, placed at a certain distance d, against the ratio $d_{obs}/\sum r_M$ (where d_{obs} is the observed interatomic distance between two next-neighbor atoms, and $\sum r_M$ is the sum of the two metallic radii),[29] where only neighboring atoms up to values $d_{obs}/\sum r_M \leq 1.25$ should be considered. The histograms for all atoms in both compounds are shown in Fig. S2 (ESI†). Since the distributions of the interatomic distances do not show clear gaps useful for the unambiguous separation of the bonding and non-bonding distances, the $d_{obs}/\sum r_M \leq 1.25$ criterion has been applied (we note that bonding/non-bonding distance differentiation is quite common in the chemistry of rare-earth compounds[30,31]). The determined coordination polyhedra around all atoms are shown in Fig. 4. In both Gd_3Ni_2 and Gd_3CoNi compounds the atomic distribution around Gd atoms indicates large and distorted polyhedra with relatively high coordination numbers, CN, of 14, 16, and 17. The coordination polyhedra for Ni1 and Ni2/Co2 are distorted tricapped trigonal prisms (CN = 9, Fig. 4). The distortion decreases with increasing Co content due to the shortening of the Gd3–Co distance.

3.3 Physical properties of Gd_3Ni_2 and $Gd_3Co_xNi_{2-x}$

Heat capacity. The heat capacity was measured between 2 and 350 K for Gd_3Ni_2 (in zero and in the applied magnetic fields

of 10, 20, 30, 40 and 50 kOe) and for $Gd_3Co_{0.5}Ni_{1.5}$ (in zero and 10 and 20 kOe fields), to check for both structural and magnetic transitions. Fig. 5a and b show the plot of the data between 80 and 240 K, respectively. The distinct λ-type peak observed in the zero field around 145 K and 150 K for Gd_3Ni_2 and $Gd_3Co_{0.5}Ni_{1.5}$, respectively, moves towards higher temperature values and broadens substantially under the applied magnetic field. Overall the two effects indicate a magnetic ordering of the ferromagnetic type in these compounds.

Magnetic properties. The temperature dependence of the magnetization, $M(T)$, was measured in applied magnetic fields of 200 Oe and 2 kOe for Gd_3Ni_2 and $Gd_3Co_xNi_{2-x}$ (for $x = 0.50$, 0.75, 0.85, 0.95, 1.00); most of the data have been collected upon warming of zero-field-cooled (ZFC) and upon field-cooling (FC) (Fig. 6 and Fig. S3, ESI†). All alloys exhibit analogous magnetic behavior: a transition from paramagnetic to ferromagnetic state manifested by a sharp increase of the $M(T)$ curves below ≈ 190 K. No thermal hysteresis was observed between the ZFC and FC curves, suggesting the transition to be of second order. The Curie temperatures, T_C, were determined from the minima of the first derivatives of M *vs.* T, dM/dT, using the data at $H = 2$ kOe; the T_C values are reported in Table 4. The T_C values increase with the Co content from 147 K in Gd_3Ni_2 to 176 K in Gd_3CoNi. The increase of the T_C values is supported by theoretical calculations (Section 3.4). The reciprocal magnetic susceptibility, $1/\chi$, under applied magnetic fields of 2 kOe for Gd_3Ni_2, Gd_3CoNi and the $Gd_3Co_xNi_{2-x}$ phases, is shown in Fig. 6a, b and Fig. S3 (ESI†) (right side of the graphs), respectively. In the paramagnetic region $1/\chi$ follows the
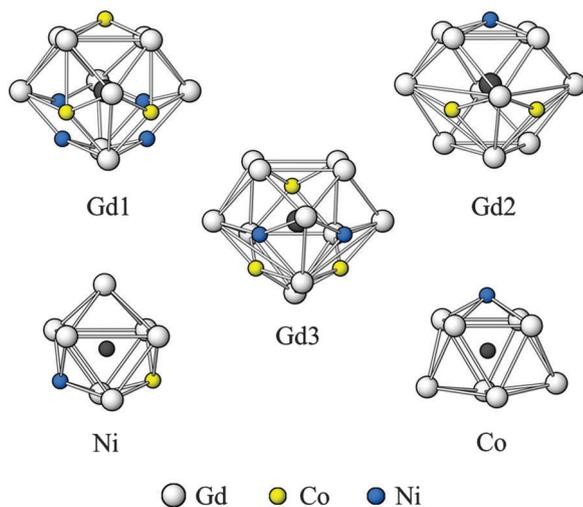

Fig. 4 Coordination polyhedra of the Gd, Co and Ni atoms in the Gd_3CoNi compound (for interatomic distances $d_{obs}/\sum r_M \leq 1.25$).
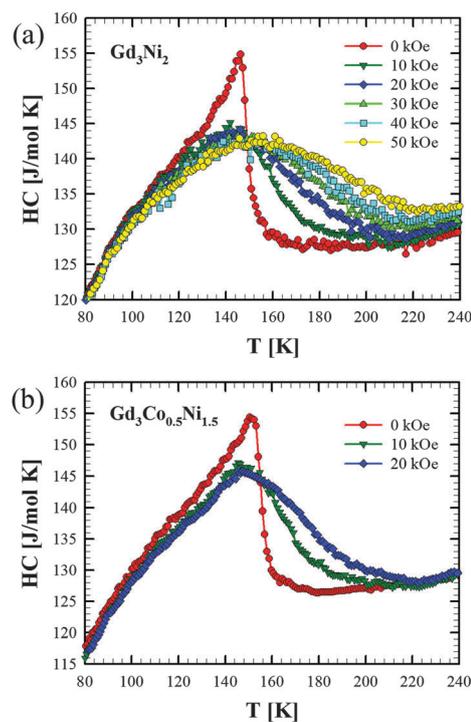

Fig. 5 Heat capacity data *vs.* temperature in the range of 80–240 K, measured in zero and applied magnetic fields of 10, 20, 30, 40, 50 kOe for Gd_3Ni_2 (a) and 10 and 20 kOe for $Gd_3Co_{0.5}Ni_{1.5}$ (b).
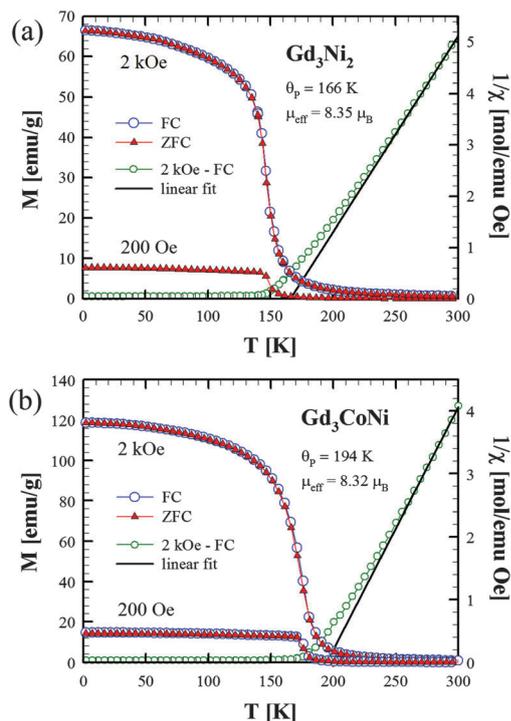
Fig. 6 Magnetization and inverse magnetic susceptibility measured in the range of 2–300 K and at 200 and 2000 Oe of Gd_3Ni_2 (a) and Gd_3CoNi (b).
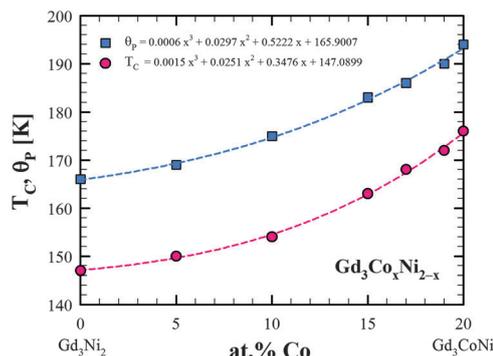

Fig. 7 The variation of the Curie temperature (T_C) and the Pauli paramagnetic temperature (θ_P) as a function of the Co content in the $Gd_3Co_xNi_{2-x}$ compounds; the dashed lines are fits to a cubic polynomial function.

Curie–Weiss law: $\chi = C/(T - \theta_P)$. A least-squares fit to the data between 220 and 300 K gives a positive Pauli paramagnetic temperature, θ_P, which agrees with the ferromagnetic ordering of these compounds (Table 4). The values of both T_C and θ_P can be fitted by a cubic function of the Co content (Fig. 7); it may be used to calculate T_C values for any intermediate composition not examined. From the Curie–Weiss fits, the experimental values of the effective magnetic moments, μ_{eff}, for all these compounds have been derived; these data are listed in Table 4. The values, ranging between 8.3 and 8.4 μ_B per Gd, are larger than the theoretical value of 7.94 μ_B for the free Gd^{3+} ion;[32] however, values of the effective moment in the paramagnetic state larger than what is expected for only the trivalent Gd ion are not uncommon. Values of μ_{eff} in excess by ≈ 0.5 μ_B were found for example in GdNi (8.5 μ_B[33–35] and 8.23 μ_B[36]); such an excess moment may arise from the polarization of the Ni-3d band induced by the Gd moment.

The isothermal magnetization, $M(H)$, was measured at 2, 5, 10 and 120 K for Gd_3Ni_2 (Fig. 8a shows the data at 5 and 120 K) and at 5 K for Gd_3CoNi (Fig. 8b) and the $Gd_3Co_xNi_{2-x}$ phases for $x = 0.50, 0.75, 0.85, 0.95$ (Fig. S4, ESI†), in fields up to 70 kOe. At 5 K, well below the T_C, the hysteresis loops for all these phases are characteristic of soft ferromagnets, with negligible a remanence and a coercive field (H_C of 5–10 Oe). For Gd_3Ni_2 the magnetization saturates at 8 kOe, with a saturation moment of 7.0 μ_B per Gd; for the substituted $Gd_3Co_xNi_{2-x}$ the magnetization is already almost saturated at a field of 5–6 kOe. The saturation moments in the Co containing phases sensibly, and progressively, increase from 7.0 to about
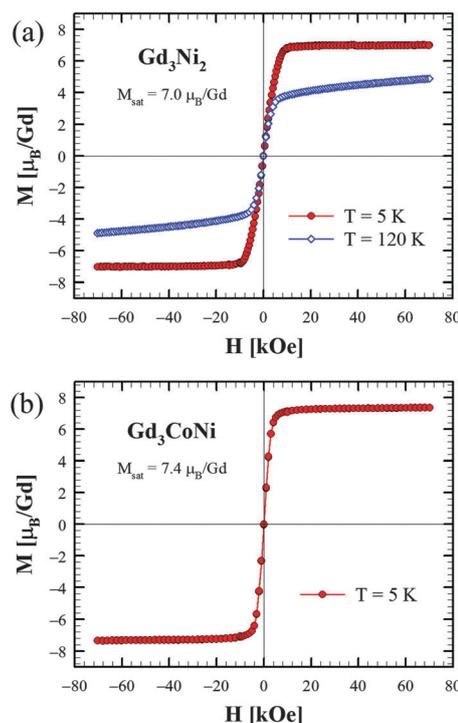
Fig. 8 Isothermal magnetization data as a function of applied magnetic field (up to 70 kOe) for Gd_3Ni_2 (at 10 and 120 K) (a) and Gd_3CoNi (at 5 K) (b) compounds.

Table 4 Magnetic properties data for Gd_3Ni_2 and $Gd_3Co_xNi_{2-x}$ compounds (with $x = 0.25, 0.50, 0.75, 0.85, 0.95, 1.00$). Saturation moment values (M_{sat}) have been obtained for measurements at $T = 5$ K

Compound	Co [at%]	T_C [K]	θ_P [K]	μ_{eff} [μ_B]	M_{sat}^a [μ_B per Gd]	M_{sat} ($H \to \infty$)^b [μ_B per Gd]
Gd_3Ni_2	0	147	166	8.35	7.00	7.0
$Gd_3Co_{0.25}Ni_{1.75}$	5	150	169	8.37	7.00	7.0
$Gd_3Co_{0.5}Ni_{1.5}$	10	154	175	8.30	7.18	7.2
$Gd_3Co_{0.75}Ni_{1.25}$	15	163	183	8.39	7.47	7.5
$Gd_3Co_{0.85}Ni_{1.15}$	17	168	186	8.44	7.44	7.5
$Gd_3Co_{0.95}Ni_{1.05}$	19	172	190	8.44	7.43	7.5
Gd_3CoNi	20	176	194	8.32	7.37	7.5

^{a} Values for a field $H = 70$ kOe. ^{b} Extrapolated values.

6084 | J. Mater. Chem. C, 2016, 4, 6078–6089

This journal is © The Royal Society of Chemistry 2016

7.4 μ_B per Gd (Table 4). While the saturation moment found for Gd_3Ni_2 corresponds to the theoretical value of the free Gd^{3+} ion, the values for the substituted $Gd_3Co_xNi_{2-x}$ compounds are slightly higher resulting from 3d–5d hybridization.

Magnetocaloric effect. Several features are required in a magnetic material for application in magnetic refrigeration, *i.e.* a Curie temperature in the vicinity of the working temperature, a large magnetic entropy change over the entire temperature range of the cycle, an almost zero magnetic hysteresis, a reasonable thermal conductivity coupled with large electrical resistance (to ensure rapid heat exchange and avoid eddy current losses), a large adiabatic temperature change, and an easy processability for the fabrication of regenerators with the desired shape.[3] The soft ferromagnetism of the title compounds, the absence of magnetic hysteresis and the nearly perfect reversibility of the magnetic transition, prompted us to investigate the magnetocaloric effect (MCE).[2,37] The MCE in Gd_3Ni_2, Gd_3CoNi, and two of the intermediate compounds ($Gd_3Co_{0.75}Ni_{1.25}$ and $Gd_3Co_{0.85}Ni_{1.15}$) was calculated in terms of the isothermal magnetic entropy change ($-\Delta S_M$) from isothermal magnetic measurements performed at several temperatures below and above the T_C in the ranges of 110–190 K for Gd_3Ni_2 (Fig. 9a), 125–225 K for Gd_3CoNi (Fig. 9b), 110–200 K for $Gd_3Co_{0.75}Ni_{1.25}$ and 130–210 K for $Gd_3Co_{0.85}Ni_{1.15}$ (Fig. S5a and b, respectively, ESI†) and in magnetic fields up to 50 kOe. The isothermal magnetic entropy change has been determined from the magnetization data using the Maxwell relation:[3,37,38]

$$\Delta S_M(T, \Delta H) = \int_0^H (\partial M/\partial T)_H dH$$

The temperature dependence of the magnetic entropy change for magnetic field changes (ΔH) of 10, 20, 30, 40 and 50 kOe in Gd_3Ni_2 and Gd_3CoNi is shown in Fig. 10a and b, respectively (Fig. S5e and f for $Gd_3Co_{0.75}Ni_{1.25}$ and $Gd_3Co_{0.85}Ni_{1.15}$, respectively, ESI†). In all compounds, the maximum value of $-\Delta S_M$ is observed around the T_C. The magnetocaloric effect increases slightly with increasing Co content: from 2.1 J kg^{-1} K^{-1} in Gd_3Ni_2 to 2.3 J kg^{-1} K^{-1} in Gd_3CoNi for $\Delta H = 10$ kOe, or from 8.0 J kg^{-1} K^{-1} in Gd_3Ni_2 to 8.3 J kg^{-1} K^{-1} in Gd_3CoNi for $\Delta H = 50$ kOe (Table S4, ESI†). These compounds exhibit relatively large magnetic entropy changes at intermediate temperatures compared with values generally found for a second order transition. The Arrott plots of these compounds (corresponding to the isothermal magnetization measurements plotted as M^2 *vs.* the ratio H/M)[39] show a positive slope around the T_C (Fig. 9c, d and Fig. S5c, d, ESI†), thereby confirming a second order transition in these phases. The magnetic entropy change as a function of the applied magnetic field increases nearly proportionally to $H^{2/3}$, as expected from the mean field theory (Fig. 11).

The magnetic entropy change is not the only parameter to characterize the potential of a magnetic refrigerant: the refrigerant capacity (RC), or cooling power,[40] is another often employed important variable. The refrigerant capacity quantifies the efficiency of a magnetic material in terms of the energy transfer between the cold and the hot reservoir in an ideal thermodynamic refrigeration cycle. It measures how much heat can be transferred between the hot and the cold ends; so, for practical applications, a large RC over a wide temperature range coupled with a
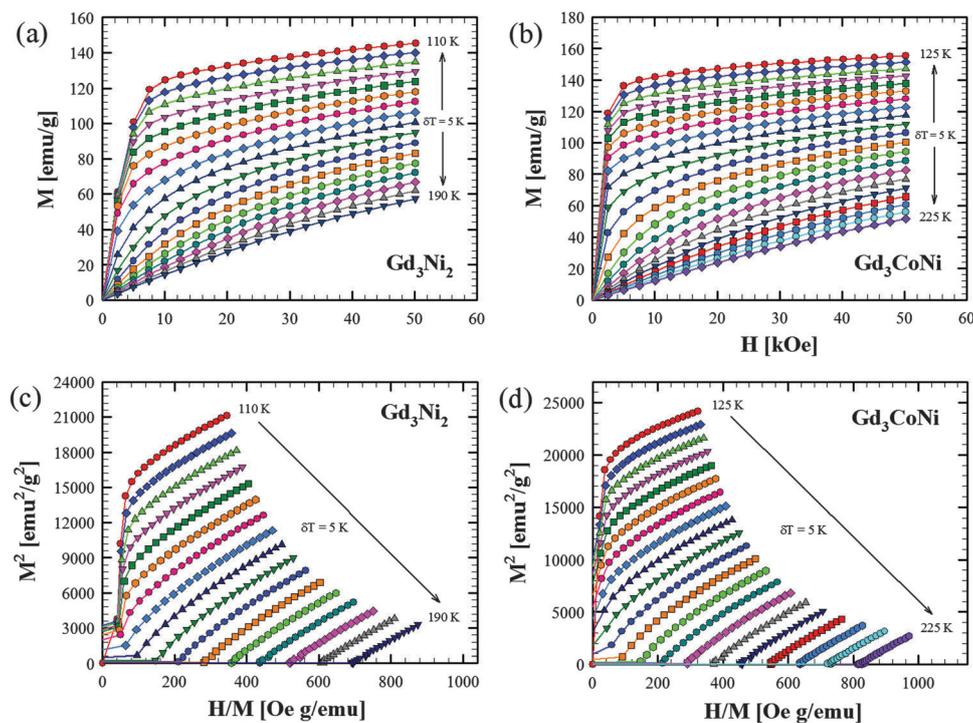

Fig. 9 Isothermal magnetization measured at selected temperatures around the magnetic transition (δT steps of 5 K) for Gd_3Ni_2 (a) and Gd_3CoNi (b) compounds; the corresponding Arrott plots for Gd_3Ni_2 (c) and Gd_3CoNi (d).
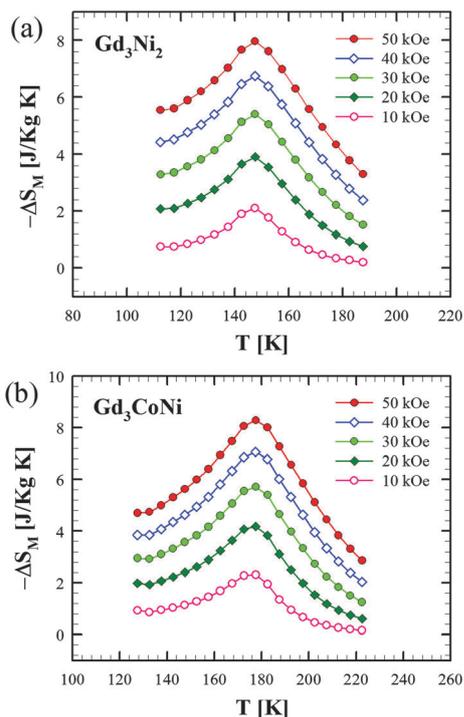
This journal is © The Royal Society of Chemistry 2016

J. Mater. Chem. C, 2016, **4**, 6078–6089 | **6085**

Fig. 10 Temperature dependence of the magnetic entropy change ($-\Delta S_M$) in Gd$_3$Ni$_2$ (a) and Gd$_3$CoNi (b) for ΔH = 10, 20, 30, 40, 50 kOe.

substantial magnetocaloric effect is desirable. For the Gd$_3$Ni$_2$, Gd$_3$Co$_{0.75}$Ni$_{1.25}$, Gd$_3$Co$_{0.85}$Ni$_{1.15}$ and Gd$_3$CoNi compounds, the RC values have been calculated by integrating the area of the $-\Delta S_M$ vs. T curves (between T1 and T2) by using the following equation:[40]

$$ RC = \int_{T1(\text{cold})}^{T2(\text{hot})} |\Delta S_M| \, dT $$

where $T1$ and $T2$ correspond to the temperatures of the hot and cold reservoir, respectively, of the system. Assuming that $T1$ and $T2$ represent the low and high temperatures, respectively, at full width at half maximum (FWHM) of $-\Delta S_M(T)$, RC$_{FWHM}$ values obtained for field changes ΔH = 10, 20, 30, 50 kOe are listed in Table S4 (ESI†). The refrigerant capacity slightly
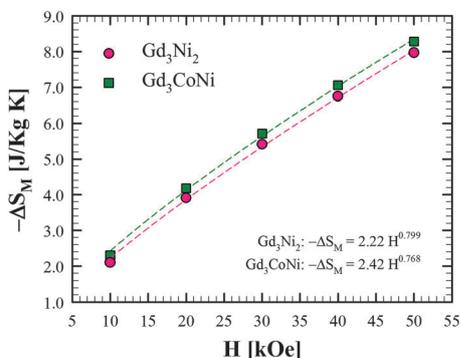

Fig. 11 Maximum isothermal magnetic entropy change ($-\Delta S_M$ at T_C) vs. the applied magnetic field for Gd$_3$Ni$_2$ and Gd$_3$CoNi.

increases with the Co content: the values range from 276 J kg^{-1} for Gd$_3$Ni$_2$ to 298 J kg^{-1} for Gd$_3$CoNi for a ΔH = 30 kOe, while the values are of the order of about 540 J kg^{-1} for ΔH = 50 kOe.

It may also be interesting to compare the magnetocaloric properties of Gd$_3$Ni$_2$ and Gd$_3$Co$_x$Ni$_{2-x}$ compounds with those of other potential magnetic refrigerants. The magnetic entropy change, $-\Delta S_M$, of these materials of $\approx$ 4.0 J kg^{-1} K^{-1} for ΔH = 20 kOe is slightly smaller than that reported for Gd metal (5.1 J kg^{-1} K^{-1}; T_C = 298 K), or the dialumide GdAl$_2$ (4.2 J kg^{-1} K^{-1}, T_C = 167 K)[41] and much smaller than that of Gd$_5$Si$_2$Ge$_2$ (14.1 J kg^{-1} K^{-1}, T_C = 299 K)[42] for the same field change of 20 kOe. At the same time, this value is higher than that observed in other Gd-based intermetallics, such as Gd$_3$Al$_2$ (3.6 J kg^{-1} K^{-1} for ΔH = 11 kOe; T_C = 281),[43] Gd$_7$Pd$_3$ (2.5 J kg^{-1} K^{-1} for ΔH = 20 kOe; T_C = 323 K)[44] and GdScGe (1.45 J kg^{-1} K^{-1} for ΔH = 15 kOe; T_C = 350 K)[45]. On the other hand, the values of refrigerant capacity observed for Gd$_3$Ni$_2$ and Gd$_3$CoNi are 153 and 180 J kg^{-1}, respectively, for a ΔH = 20 kOe (540 and 545 J kg^{-1}, respectively, for a ΔH = 50 kOe). These values compare favorably with other RC$_{FWHM}$ data reported for most Gd intermetallics with a T_C around room temperature, but are even higher than for compounds with a lower T_C, thus making them potential candidates for intermediate-temperature magnetic refrigerant materials.

3.4 Theoretical calculations

Local spin density approximation including onsite electron correlation (LSDA+U)[46] calculations have been performed for Gd$_3$Ni$_2$ and Gd$_3$CoNi, in conjunction with the tight-binding linear muffin-tin orbital and full-potential linear augmented plane wave band structure methods.[47,48] k-space integrations have been performed with $32 \times 32 \times 32$ Brillouin zone mesh for the convergence of total charge and total energy. Since the 4f states are half filled in the Gd atoms of the two compounds, the LSDA+U (with U = 6.7 eV and J = 0.7 eV) is considered to be the best approach for the correct positioning of occupied and unoccupied 4f states by shifting occupied 4f states below the Fermi level and unoccupied 4f states above the Fermi level. The total energy calculations were initially performed for Gd$_3$CoNi using the atomic coordinates of Gd$_3$Ni$_2$ (Dy$_3$Ni$_2$-type; Table 3); they predicted a lower total energy (by 31.3 meV per cell) by positioning the Co atom in the Ni2 position [in (0.24231, 0, 0.22675)] compared to that with the Co atom in the Ni1 position [in (0.03578, 0, 0.14319)]. This indicates that the Ni2 position is preferred by Co. The calculations were repeated later using the crystallographic parameters as obtained from single crystal X-ray diffraction; again, they confirmed a similar energy difference (27.9 meV per cell) and the same conclusion about the preferential Ni and Co site occupancies.

Fig. 12 shows atom projected 4f, 5d and 3d density of states of Gd$_3$Ni$_2$ and Gd$_3$CoNi. The energy-band centers of occupied 4f density of states (DOS) of the three non-equivalent Gd atoms (Fig. 12a and d) slightly change when Ni at the Ni2 site of Gd$_3$Ni$_2$ is replaced by Co. This is likely due to the slight change in the Gd positions and, consequently, in the Gd–Gd distances while substituting Ni2 by Co. The unoccupied 4f DOS in both
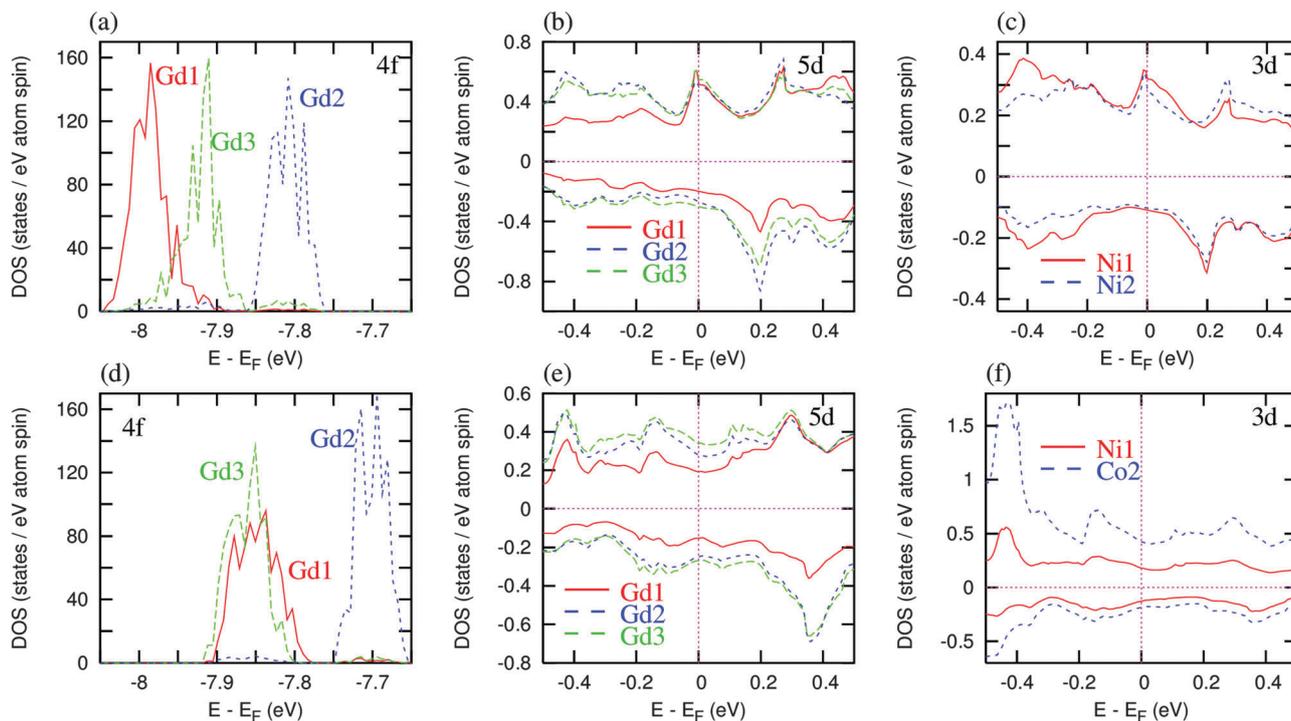
6086 | J. Mater. Chem. C, 2016, 4, 6078–6089

This journal is © The Royal Society of Chemistry 2016

Fig. 12 (a) and (d) Gd 4f, (b) and (e) Gd 5d, and (c) and (f) Ni/Co 3d density of states (DOS) of Gd_3Ni_2 and Gd_3CoNi compounds, respectively.

compounds is ≈ 4 eV above the Fermi level (not shown). The 5d DOS of non-equivalent Gd atoms in Gd_3Ni_2 is exchange-split by ≈ 0.2 eV between spin-up and spin-down 5d states across the Fermi level (Fig. 12b). Identical exchange splitting across the Fermi level is also observed in the 3d density of states of Ni atoms in Gd_3Ni_2 (Fig. 12c). This indicates that the Gd 5d and Ni 3d bands are hybridized in this compound. The Ni 3d magnetic moments are less than 0.03 μ_B, *i.e.* they are negligible compared to the Gd 5d moments. The magnetic moments of the three non-equivalent Gd1, Gd2, and Gd3 in Gd_3Ni_2 are 7.36 μ_B, 7.45 μ_B, and 7.47 μ_B, respectively. The ≈ 7 μ_B are from 4f moments and the remaining are from spin polarized 5d electrons due to the indirect 4f–4f exchange interactions. On the other hand, in Gd_3CoNi the calculations show an exchange splitting of ≈ 0.5 eV between spin-up and spin-down Gd 5d and Ni/Co 3d states across the Fermi level (Fig. 12e and f). The Gd1, Gd2, Gd3 and Ni1 magnetic moments essentially remain identical to those of Gd_3Ni_2. Although Co moments (-0.34 μ_B) align antiparallel to Gd moments as expected, the enhanced Gd 5d and Ni/Co 3d exchange splitting at the Fermi level supports the experimentally observed enhancement of the Curie temperature in Gd_3CoNi compared to Gd_3Ni_2 and may account for a larger than expected moment.

4 Conclusions

The existence of the stoichiometric intermetallic compound Gd_3Ni_2 has been confirmed; it is a high temperature phase, which forms by a peritectic reaction at 988 K and decomposes

below ≈ 923 K. The compound crystallizes in the monoclinic Dy_3Ni_2 structure type [$mS20$, $C2/m$ (No. 12), $Z = 4$] with lattice parameters [$a = 13.418(3)$ Å, $b = 3.720(1)$ Å, $c = 9.640(2)$ Å, $\beta = 106.250(3)°$]. Ni in Gd_3Ni_2 can be substituted by Co up to 50% to form the $Gd_3Co_xNi_{2-x}$ pseudo-binary compounds (up to Gd_3CoNi, for $x = 1.0$) while preserving the same monoclinic structure of the binary Co-free parent. Substitution stabilizes the $Gd_3Co_xNi_{2-x}$ phases down to room temperature. For higher Co content the structure changes to the orthorhombic Y_3Co_2-type [$oP20$, $Pnnm$, (No. 58), $Z = 4$], which is related to the Dy_3Ni_2 prototype *via* a shear distortion. The Gd_3CoNi compound, corresponding to the Co-rich limit of the monoclinic solid solution $Gd_3Co_xNi_{2-x}$, has been found to be a true stoichiometric ternary compound; its structure represents a new ternary proto-type, an ordered derivative of the Dy_3Ni_2-type. Chemical and geometrical considerations, along with theoretical calculations, suggest site-occupancy preference for Co atoms in only one of the two available 4i Wyckoff sites occupied by Ni in Gd_3Ni_2. Single crystal investigation of Gd_3CoNi confirms the ordered atomic arrangement of Co and Ni in two distinct crystallographic sites. To the best of our knowledge, this is the first example of an intermetallic phase containing both Co and Ni showing ordered site occupations by the two atoms.

Both Gd_3Ni_2 and Co-substituted phases exhibit similar magnetic behaviors: a long range ferromagnetic order sets in at T_C values progressively increasing from 147 K (for Gd_3Ni_2) to 176 K (for Gd_3CoNi). Saturation moments of 7.0 μ_B per Gd for Gd_3Ni_2 and 7.0–7.4 μ_B per Gd for the $Gd_3Co_xNi_{1-x}$ phases have been found. The increase in the saturation magnetic moment from Gd_3Ni_2 to Gd_3CoNi reflects the enhanced contribution

This journal is © The Royal Society of Chemistry 2016

J. Mater. Chem. C, 2016, **4**, 6078–6089 | **6087**

from 5d electrons of Gd. Reversible and soft ferromagnetism of these compounds, with negligible hysteresis, makes these new Gd-based intermetallics potentially useful magnetic refrigerant materials at intermediate temperatures.

Total energy calculations confirm the observed crystallographic site preference of Co and Ni atoms in Gd_3CoNi. The enhanced Gd 5d and Ni/Co 3d exchange splitting at the Fermi level supports the experimentally observed enhanced Curie temperature in Gd_3CoNi compared to that of Gd_3Ni_2. These new compounds constitute a potentially interesting source for investigation in both theoretical and experimental research. These new phases deserve further investigation to probe the effect of Gd substitution by another R (e.g. Nd) and/or Ni by a different transition metal (or a p-block element), with the aim of either tuning the T_C or enhancing the MCE.

Acknowledgements

References

1 V. Franco, J. S. Blázquez, B. Ingale and A. Conde, *Annu. Rev. Mater. Res.*, 2012, **42**, 305–342.

2 K. A. Gschneidner Jr, V. K. Pecharsky and A. O. Tsokol, *Rep. Prog. Phys.*, 2005, **68**, 1479–1539.

3 A. M. Tishin and Y. I. Spichkin, The magnetocaloric effect and its applications, *Series of Condensed Matter Physics*, Institute of Physics publishing, Bristol, 2003.

4 T. B. Massalski, *Binary Alloy Phase Diagrams*, ASM International, Metals Park, OH, 2nd edn, 1990.

5 P. Villars and L. D. Calvert, *Pearson's Handbook of Crystallographic Data for Intermetallic Compounds*, ASM International, Metals Park, OH, 2nd edn, 1991.

6 P. Villars, K. Cenzual, *Pearson's Crystal Data – Crystal Structure Database for Inorganic Compounds*, ASM International, Materials Park, OH, Release 2010/11.

7 M.I. Copeland, M. Krug, C.E. Armantrout, H. Kato, *Report of Investigations* 6566, Bureau of Mines, US-DOI, 1964.

8 V. F. Novy, R. C. Vickery and E. V. Kleber, *Trans. Metall. Soc. AIME*, 1961, **221**, 585–588.

9 G. Xu, Y.-W. Cui, H. Fei, L. Zhang, F. Zheng, L. Liu and Z. Jin, *Int. J. Mater. Res.*, 2012, **103**, 1179–1187.

10 J. M. Moreau, D. Paccard and E. Parthé, *Acta Crystallogr., Sect. B: Struct. Crystallogr. Cryst. Chem.*, 1974, **30**, 2583–2586.

11 J. M. Moreau, D. Paccard and D. Gignoux, *Acta Crystallogr., Sect. B: Struct. Crystallogr. Cryst. Chem.*, 1974, **30**, 2122–2126.

12 J. Le Roy, J. M. Moreau, D. Paccard and E. Parthé, *Acta Crystallogr., Sect. B: Struct. Crystallogr. Cryst. Chem.*, 1977, **33**, 3406–3409.

13 A. Provino, P. Manfrinetti, V. Smetana, M. Putti, D. Paudyal and K. A. Gschneidner Jr, *American Physical Society 2014 Conference*, Denver (CO), March 3–7, 2014.

14 Materials Preparation Center, The Ames Laboratory, US Department of Energy, Ames, IA, USA, www.mpc.ameslab.gov.

15 K. Yvon, W. Jeitschko and E. Parthé, *J. Appl. Crystallogr.*, 1977, **10**, 73–74.

16 *SAINT Program*, Siemens Analytical X-ray Instruments Inc., Madison, WI, 1996.

17 *SHELXTL*, Bruker AXS, Inc., Madison WI, 2000.

18 A. Altomare, M. C. Burla, M. Camalli, G. L. Cascarano, C. Giacovazzo, A. Guagliardi, A. G. G. Moliterni, G. Polidori and R. Spagna, *J. Appl. Crystallogr.*, 1999, **32**, 115–119.

19 G. M. Sheldrick, *Acta Crystallogr., Sect. A: Found. Crystallogr.*, 2008, **64**, 112–122.

20 V. K. Pecharsky, J. O. Moorman and K. A. Gschneidner Jr, *Rev. Sci. Instrum.*, 1997, **68**, 4196–4207.

21 P. Villars and J. L. C. Daams, *J. Alloys Compd.*, 1993, **197**, 177–196.

22 J. M. Moreau, E. Parthé and D. Paccard, *Acta Crystallogr., Sect. B: Struct. Crystallogr. Cryst. Chem.*, 1975, **31**, 747–749.

23 W. B. Pearson, *The Crystal Chemistry and Physics of Metals and Alloys*, Wiley-Interscience, New York, 1972.

24 O. Kubaschewski, C. B. Alcock and P. J. Spencer, *Materials Thermochemistry*, Pergamon Press, Oxford, 6th edn, 1993.

25 K. A. Gschneidner Jr, *Met., Mater. Processes*, 1990, **1**, 241–251.

26 J. L. C. Daams, P. Villars and J. H. N. van Vucht, *Atlas of Crystal Structure Types for Intermetallic Phases*, ASM International, Materials Park, OH, 1991, vol. 1.

27 W. C. Hamilton, *Acta Crystallogr.*, 1965, **18**, 502–510.

28 E. Teatum, K. A. Gschneidner Jr and J. Waber, *Rep LA-4003*, NTIS, Springfield, VA, 1968.

29 G. Bruzzone, M. L. Fornasini and F. Merlo, *J. Less-Common Met.*, 1970, **22**, 253–264.

30 M. L. Fornasini, A. Mugnoli and A. Palenzona, *Acta Crystallogr., Sect. B: Struct. Crystallogr. Cryst. Chem.*, 1979, **35**, 1950–1953.

31 F. Canepa, S. Cirafici, M. L. Fornasini, P. Manfrinetti, F. Merlo, A. Palenzona and M. Pani, *J. Alloys Compd.*, 2000, **297**, 109–113.

32 *Handbook on the Physics and Chemistry of Rare Earths*, ed. K. A. Gschneidner Jr and L. Eyring, North-Holland Physics Publishing, Amsterdam, 1978, vol. 1.

33 J. A. Blanco, J. C. Gomez Sal, J. Rodriguez Fernandez, D. Gignoux, D. Schmitt and J. Rodriguez-Carvajal, *J. Phys.: Condens. Matter*, 1992, **4**, 8233–8244.

34 P. L. Paulose, S. Patil, R. Mallik, E. V. Sampathkumaran and V. Nagarajan, *Physica B*, 1996, **223** and **224**, 382–384.

35 R. Mallik, P. L. Paulose, E. V. Sampathkumaran, S. Patil and V. Nagarajan, *Phys. Rev. B: Condens. Matter Mater. Phys.*, 1997, **55**, 8369–8373.

36 D. Paudyal, Y. Mudryk, Y. B. Lee, V. K. Pecharsky, K. A. Gschneidner Jr and B. N. Harmon, *Phys. Rev. B: Condens. Matter Mater. Phys.*, 2008, **78**, 184436.

6088 | *J. Mater. Chem. C*, 2016, **4**, 6078–6089

This journal is © The Royal Society of Chemistry 2016

37 V. K. Pecharsky and K. A. Gschneidner Jr, *J. Magn. Magn. Mater.*, 1999, **200**, 44–56.

38 A. H. Morrish, *The Physical Principles of Magnetism*, Wiley, New York, 1965.

39 S. K. Banerjee, *Phys. Lett.*, 1964, **12**, 16–17.

40 K. A. Gschneidner Jr, V. K. Pecharsky, A. O. Pecharsky and C. B. Zimm, *Mater. Sci. Forum*, 1999, **315–317**, 69–76.

41 V. K. Pecharsky and K. A. Gschneidner Jr, *Adv. Cryog. Eng.*, 1996, **42**, 423–428.

42 V. K. Pecharsky and K. A. Gschneidner Jr, *Phys. Rev. Lett.*, 1997, **78**, 4494–4497.

43 V. K. Pecharsky, K. A. Gschneidner Jr, S. Y. Dan′kov and A. M. Tishin, *Cryocoolers*, 2002, **10**, 639–645.

44 F. Canepa, M. Napoletano and S. Cirafici, *Intermetallics*, 2002, **10**, 731–734.

45 S. Couillaud, E. Gaudin, V. Franco, A. Conde, R. Pöttgen, B. Heying, U. C. Rodewald and B. Chevalier, *Intermetallics*, 2011, **19**, 1573–1578.

46 V. I. Anisimov, F. Aryasetiawan and A. I. Lichtenstein, *J. Phys.: Condens. Matter*, 1997, **9**, 767–808.

47 O. K. Andersen and O. Jepsen, *Phys. Rev. Lett.*, 1984, **53**, 2571–2574.

48 P. Blaha, K. Schwarz, G. Madsen, D. Kvasnicka and J. Luitz, *Wien2k, an augmented plane wave + local orbitals program for calculation crystal properties*, Karlheinz Schwarz Tech. Universität, Wien, 2001.

This journal is © The Royal Society of Chemistry 2016

J. Mater. Chem. C, 2016, **4**, 6078–6089 | **6089**